Int. J. Appl. Math. Comput. Sci., 2019, Vol. 29, No. 2, 285–303
DOI: 10.2478/amcs-2019-0021

A NEW EFFICIENT ADAPTIVE CONTROL OF TORSIONAL VIBRATIONS INDUCED BY SWITCHED NONLINEAR DISTURBANCES

MACIEJ WASILEWSKI [a,*], DOMINIK PISARSKI [a], ROBERT KONOWROCKI [a], CZESŁAW I. BAJER [a]

[a] Institute of Fundamental Technological Research
Polish Academy of Sciences, Pawińskiego 5B, 02-105 Warsaw, Poland
e-mail: mwasil@ippt.pan.pl

Torsional vibrations induced in drilling systems are detrimental to the condition of the machine and to the effectiveness of the engineering process. The cause of vibrations is a nonlinear and unknown friction between a drill string and the environment, containing jumps in its characteristics. Nonlinear behaviour of the friction coefficient results in self-excited vibration and causes undesirable stick-slip oscillations. The aim of this paper is to present a novel adaptive technique of controlling vibrating systems. The scheme is based on the linear quadratic regulator and uses direct measurements of the friction torque to synthesize its linear dynamic approximation. This approach allows generating a control law that takes into account the impact of the friction on the system dynamics and optimally steers the system to the desired trajectory. The controller's performance is examined via numerical simulations of the stabilization of the drilling system. The proposed solution outperforms the comparative LQG regulator in terms of the minimization of the assumed cost functional and the overall stability of the control system under the nonlinear disturbance.

Keywords: vibration control, adaptive control, linear-quadratic-regulator, drilling control.

1. Introduction

The problem of vibration attenuation is present in many branches of modern engineering. Bridges and railway tracks vibrate under moving vehicles, which can damage the structure as well as neighboring objects. Robotic manipulators are required to act at high speeds, and the use of light, flexible links results in vibrations of the robotic joint, which worsens the precision of the motion. The vibrations induced in machine tools, such as lathes and grinding machines, reduce the accuracy of the shape of the manufactured object and can also damage the machine.

Extensive literature deals with vibration control. It can be divided into the development of specific hardware and control methods. A survey of the actuators developed for vibration control is provided by Symans and Constantinou (1999). Apart from hardware development, research into control algorithms for vibrating systems is also very intensive. An input shaping scheme for controlling a two-link flexible arm robot is presented by Hillsley and Yurkovich (1991). Tzes and Yurkovich (1993) use input shaping with adaptive precompensation to control systems with unknown parameters. Negative input shapers for the control of a flexible arm robot are presented by Mohamed *et al*. (2006). Singhose (2009) presents a comprehensive review of command shaping for flexible systems. The control of a vibrating beam obtained by the use of an optimal control framework with an H_∞ filter is presented by Li *et al*. (1994). An open-loop optimal control for damping the forced vibrations of a beam is discussed by Kucuk *et al*. (2013). Pisarski and Bajer (2010) propose a semi-active control of an elastic continuum under a travelling load.

Apart from open-loop algorithms, the domain of vibration suppression uses feedback controllers. Robust H_∞ controllers for vibration control problems are described by Kar *et al.* (2000a; 2000b). The optimal control approach for vibration damping in rotational systems using semi-active dampers is investigated by Michajłow *et al*. (2017). In the work of Bajer *et al*. (2017) the usage of a controllable viscous damping layer with an optimal control law for vibration mitigation of the plate subjected to a pair of masses moving in

*Corresponding author

opposite directions is considered. Adaptive suboptimal stabilization of the beam under moving load by the use of controllable dampers is proposed by Pisarski and Myśliński (2017). An interesting sliding-mode control for vibration mitigation in mechanical systems based on the polar coordinate approach is presented by Young (1998).

In the present paper, we demonstrate a novel adaptive optimal control scheme for mechanical vibrating systems induced by time-varying excitation. The proposed algorithm consists of two fundamental elements, i.e., the identification part, which, based on the consecutive measurements, generates an approximated dynamical model of the excitation, and the actual control algorithm, which computes the values of the control inputs as a function of the internal state of a vibrating system and the state concerned with the aforementioned excitation model.

The proposed scheme is employed for vibration attenuation of a drilling system subjected to a change in the ground friction characteristics. The friction is considered a generalized resistance of the drilled ground to the drilling. It can be both smooth in time and stepwise variable and can contain a sudden jump of characteristics. It generates a resistive force that can change suddenly when the drill passes a layer of soil or rock or meets rigid inclusions. The voltage supplying the electric motor is the control function and, when applied to the system, it influences the dynamic response in a nonlinear way. A drill string used in drilling for gas and oil is an example of such a system. The string has a low diameter-to-length ratio. The sticking phase and the phase of slipping when the friction coefficient decreases may lead to instability of the system and to stick-slip flicker. Self-induced vibrations lower the effectiveness of the drilling process and may even damage the drill. The friction parameters depend on the rock formation, which means that the resulting friction varies with the depth of the drilling.

The solutions proposed in the literature can be divided into passive and active approaches. The former solutions focus on optimization of the drilling bit parameters or drilling input parameters, such as the weight of the drill bit, the input torque, and the rotary speed, to make stick-slip vibrations less likely to occur. This approach is presented by Davis *et al*. (2012), who proposed an increase in the torsional stiffness of the drill string and a redesign of the bit. In a work by Bailey and Remmert (2010) the optimization of the bottom hole assembly (BHA) design is reported.

One of the active methods for vibration attenuation is to optimize the aforementioned parameters in real time, based on measurements. In the work of Fear and Abbassian (1994) an automated vibration detection system with guidelines for the machine operators is proposed. In another approach, active control systems are used. In the work of Hernandez-Suarez *et al*. (2009), a sliding mode control scheme is proposed to attenuate stick-slip oscillations in oil drill strings. An active damping system based on feedback control is developed by Jansen and van den Steen (1995). Christoforou and Yigit (2003) present an active strategy based on optimal state feedback control. An H_∞ controller for a drilling system is given by Serrarens *et al*. (1998). In the work of Monteiro and Trindade (2017) a control scheme based on the proportional-integral regulator for reduction of torsional vibration in a drill string is investigated. A comprehensive review of the literature concerning vibration suppression in drilling systems is given by Zhu *et al*. (2015).

The drilling machine can be treated as a special case of a more general drive system coupled with an elastic joint. There exist numerous examples of vibration control algorithms for such systems that also deal with the disturbances explicitly. A sliding-mode control and reconstruction of the disturbance value by the Kalman filtering are proposed by Orlowska-Kowalska *et al*. (2010). Szabat *et al*. (2015) formulate a nonlinear fuzzy Luenberger observer that estimates the state of the system along with the present value of the disturbance load. A similar fuzzy disturbance observer is introduced by Wang *et al*. (2016). It can be concluded that the attention of the aforementioned papers is focused on the estimation of the disturbance *value*.

Contrarily, the goal of the present paper is to get the best estimation of the disturbance *dynamics*. Because this estimation gives insight into the future change in the load, the control law is adjusted accordingly and the control displays greater performance than in the case of knowing only the instantaneous value of the disturbance. A similar attempt is proposed by Priesner and Jakubek (2014), where model predictive control (MPC) is used and the load is incorporated in the controller as a simple dynamical model with constant parameters. In contrast to this proposal, the parameters of our disturbance model are allowed to change so that the model adapts to the measured course of the load. This adaptivity is crucial for the drilling process because the character of the friction torque can vary dramatically as the drill bit enters consecutive layers of the soil.

Although the experimental verification of the derived control method is the ultimate goal of the authors, in this paper, we rather opt for the numerical simulation. This allows us to precisely analyse the effectiveness of the scheme in dependence on its various parameters. For the simulation purposes, a simplified model of a drill string powered by a DC motor is introduced. The disturbance applied in the control consists of a nonlinear model of the friction and the Gaussian noise. The parameters of this disturbance vary for different simulation scenarios considered.

This paper is organized as follows. Section 2 provides the formulation of the problem with assumed

simplifications of the drilling system. Section 3 is devoted to the derivation of the proposed control scheme. In Section 4 the numerical simulation results are provided, consisting of the performance comparison to the linear-quadratic-Gaussian (LQG) controller and the analysis of the controller parameters.

2. Model description

Let us consider the system depicted in Fig. 1. It consists of a DC motor with resistance R_{DC}, inductance L, and electromotive force constant K_e. The motor generates the torque T_D. Although the drill string part of the machine can be modelled as a dynamical distributed parameter system that is then transformed into its lumped approximation (see Jansen and van den Steen, 1995; Kreuzer and Steidl, 2012), it is also common to model it directly by a lumped parameter system (see van de Vrande *et al*., 1999; Serrarens *et al*., 1998; Mihajlović *et al*., 2004; Hernandez-Suarez *et al*., 2009). In this paper, we employ the latter strategy and define the mechanical part of the system only by means of a set of rigid bodies. The shaft of the motor is firmly connected to the first body. The moment of inertia of this coupling is I_0. The next three bodies are numbered from left to right and are characterized by the moments of inertia denoted by I_1, I_2, I_3, respectively. These bodies are interconnected by the use of torsion springs of stiffnesses k_1, k_2 and k_3, and torsion dampers with damping coefficients c_1, c_2, and c_3. The angular displacement and angular velocity of the i-th body are denoted by ϕ_i and $\dot{\phi}_i$, respectively. The disturbance torque, consisting of the torsional friction $T_F(\dot{\phi}_3)$ and other disturbances, modelled as white noise, is assumed to excite the body I_3.

The friction torque is defined as (Kreuzer and Steidl, 2012)

$$T_F\left(\dot{\phi}_3\right) = \begin{cases} \left(T_C + [T_B - T_C]\, e^{-c_v|\dot{\phi}_3|}\right) \operatorname{sign}(\dot{\phi}_3) \\ +f_T\dot{\phi}_3 \quad \text{if } \left|\dot{\phi}_3\right| \geq \dot{\phi}_c, \\ \left(\frac{\dot{\phi}_3}{\dot{\phi}_c}\right)\left(T_C + [T_B - T_C]\, e^{-c_v\dot{\phi}_c}\right. \\ \left.+f_T\dot{\phi}_c\right) \quad \text{if } \left|\dot{\phi}_3\right| < \dot{\phi}_c, \end{cases} \tag{1}$$

where T_C is the Coulomb friction torque, T_B is the static friction torque, c_v defines the steepness of the friction characteristics, and f_T is the viscous friction coefficient. The parameter $\dot{\phi}_c$ defines the length of the interval of the angular velocity on the friction characteristics on which the sticking phase (static friction) is approximated by a straight line.

The dynamics of the mechanical coupling are represented by the second-order nonlinear differential equation

$$\mathbf{M}\ddot{\mathbf{y}} + \mathbf{C}\dot{\mathbf{y}} + \mathbf{K}\mathbf{y} = -\mathbf{F}_{\text{frict.}} T_F(\dot{\phi}_3) + \mathbf{F}_{\text{DC}} T_D(\dot{\mathbf{y}}, u), \tag{2}$$

where $\mathbf{y} = \begin{bmatrix}\phi_0 & \cdots & \phi_3\end{bmatrix}^T$ is the vector of the angular positions of the bodies while $\dot{\mathbf{y}}$ and $\ddot{\mathbf{y}}$ are the vectors of angular velocities and accelerations of the bodies, respectively. The matrix $\mathbf{M} = \operatorname{diag}(I_0, I_1, I_2, I_3)$ is the mass matrix of the system, $\mathbf{K}$ is the stiffness matrix, $\mathbf{C}$ is the damping matrix, and $\mathbf{F}_{\text{frict.}} = \begin{bmatrix}0 & 0 & 0 & 1\end{bmatrix}^T$ and $\mathbf{F}_{\text{DC}} = \begin{bmatrix}1 & 0 & 0 & 0\end{bmatrix}^T$ are the vectors allocating the nonlinear friction and motor torque on the mechanical part of the system, respectively. The dynamic behavior of the DC motor is described by the equation

$$\dot{T}_D = -\frac{K_e^2}{L}\mathbf{E}\dot{\mathbf{y}} - \frac{R}{L}T_D + \frac{K_e}{L}u, \tag{3}$$

where $\mathbf{E} = \begin{bmatrix}1 & 0 & 0 & 0\end{bmatrix}$ represents the impact of the angular velocity of the first body on the motor's torque ($\mathbf{E}\dot{\mathbf{y}} = \dot{\phi}_0$).

Both Eqns. (3) and (2) can be rewritten as the first-order differential equation that links both the mechanical and electric part of the system considered:

$$\dot{\mathbf{x}} = \mathbf{A}\mathbf{x} + \mathbf{B}u + \mathbf{D}T_F(\dot{\phi}_3), \tag{4}$$

$$\mathbf{x} = \begin{bmatrix}\mathbf{y}^T & \dot{\mathbf{y}}^T & T_D\end{bmatrix}^T, \quad \mathbf{x} \in \mathbb{R}^9, \tag{5}$$

where $\mathbf{x}$ is the state of the system that is made up of the set of angular displacements and velocities of all rigid bodies, ϕ_{0-3} and $\dot{\phi}_{0-3}$, along with the torque generated by the DC motor T_D. The control input u is assumed as the voltage applied to the DC motor and its value has to fulfill the constraints selected to guarantee

$$|u| \leq u_{\max}. \tag{6}$$

The matrix

$$\mathbf{A} = \begin{bmatrix} \mathbf{0} & \mathbf{I} & \mathbf{0} \\ -\mathbf{M}^{-1}\mathbf{K} & -\mathbf{M}^{-1}\mathbf{C} & \mathbf{M}^{-1}\mathbf{F}_{\text{DC}} \\ \mathbf{0} & -\frac{K_e^2}{L}\mathbf{E} & -\frac{R}{L} \end{bmatrix} \in \mathbb{R}^{9\times 9} \tag{7}$$

is the state-transition matrix of values defined by Eqns. (3) and (2),

$$\mathbf{B} = \begin{bmatrix}0 & \cdots & 0 & \frac{K_e}{L}\end{bmatrix}^T, \tag{8}$$

is the matrix allocating the control input in the system, defined by Eqn. (3), and

$$\mathbf{D} = \begin{bmatrix} \mathbf{0} \\ -\mathbf{M}^{-1}\mathbf{F}_{\text{frict.}} \\ 0 \end{bmatrix} = \begin{bmatrix}0 & \cdots & 0 & -\frac{1}{I_3} & 0\end{bmatrix}^T \tag{9}$$

represents the impact of the friction force.

The initial point of the system considered in the simulations is assumed to be at the origin of the state space

$$\mathbf{x}(0) = \begin{bmatrix}0 & \cdots & 0\end{bmatrix}^T. \tag{10}$$

The goal of the control is to control all bodies to yield constant angular velocity ω_d. The desired state of the

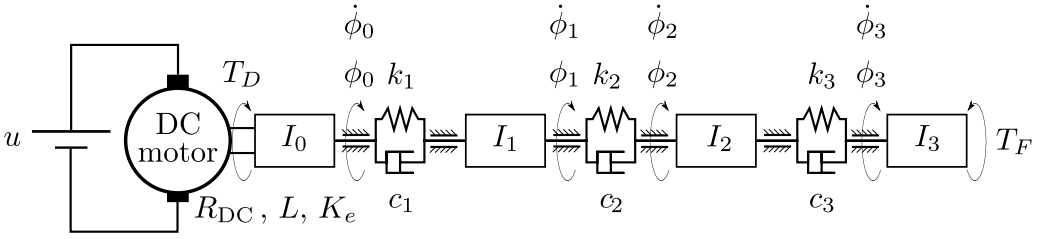

Fig. 1. Scheme of the controlled object.

system is achieved when all the bodies of the system rotate with an identical constant angular velocity ω_d. This condition is feasible only if the torque T_D generated by the motor is constant and equal to the friction torque corresponding to the velocity ω_d, i.e., $T_D = T_F(\omega_d)$. This means that the operating point to be tracked by the control

$$\begin{aligned}&\mathbf{x}_d(t)\\ &= \begin{bmatrix}\phi_0^d(t) & \cdots & \phi_3^d(t) & \dot\phi_0^d(t) & \cdots & \dot\phi_3^d(t) & T_D^d(t)\end{bmatrix}^T\end{aligned} \tag{11}$$

fulfills the condition

$$\dot{\mathbf{x}}_d(t) = \begin{bmatrix}\omega_d & \omega_d & \omega_d & \omega_d & 0 & 0 & 0 & 0 & 0\end{bmatrix}^T. \tag{12}$$

The trajectory $\mathbf{x}_d(t)$ and the value of the control at the operating point u_d are obtained from the equation

$$\dot{\mathbf{x}}_d(t) = \mathbf{A}\mathbf{x}_d(t) + \mathbf{B}u_d + \mathbf{D}T_F(\omega_d). \tag{13}$$

The solution of (13) is

$$\begin{aligned}\mathbf{x}_d(t) =& \begin{bmatrix}\omega_d t & \omega_d t + \xi_1 & \omega_d t + \xi_2 & \omega_d t + \xi_3\\ \omega_d & \omega_d & \omega_d & \omega_d & T_F(\omega_d)\end{bmatrix}^T,\\ u_d =& \frac{RT_F(\omega_d) + K_e^2\omega_d}{K_e}.\end{aligned} \tag{14}$$

The identity $T_D^d = T_F(\omega_d)$ means that the value of the torque generated by the motor at the operating point has to be equal to that of the friction torque at the angular velocity setpoint. Since the system of the bodies at the operating point acts under two opposite torques, a static stretch between the bodies appears. The presence of this phenomenon is reflected in the reference trajectory by the occurrence of the ξ_i terms. These are equal to the static difference between the angular position of the first body and the i-th body at the operating point and are represented as

$$\begin{aligned}\xi_1 &= -T_F(\omega_d)\frac{1}{k_1},\\ \xi_2 &= -T_F(\omega_d)\frac{k_1 + k_2}{k_1 k_2},\\ \xi_3 &= -T_F(\omega_d)\frac{k_1k_2 + k_2k_3 + k_3k_2}{k_1k_2k_3}.\end{aligned} \tag{15}$$

The error state-space representation of the system can be introduced as

$$\boldsymbol{\epsilon}(t) = \mathbf{x}(t) - \mathbf{x_d}(t). \tag{16}$$

It can be noticed that the error dynamical equation is analogous to the system equation (4):

$$\dot{\boldsymbol{\epsilon}} = \mathbf{A}\boldsymbol{\epsilon} + \mathbf{B}u_\epsilon + \mathbf{D}T_F^\epsilon(\dot\epsilon_3), \tag{17}$$

$$u_\epsilon(t) = u(t) - u_d, \tag{18}$$

$$\begin{aligned}\boldsymbol{\epsilon}(0) =& -\mathbf{x_d}(0)\\ =& \begin{bmatrix}0 & -\xi_1 & -\xi_2 & -\xi_3 & -\omega_d\\ & -\omega_d & -\omega_d & -\omega_d & -T_F(\omega_d)\end{bmatrix}^T,\end{aligned} \tag{19}$$

$$T_F^\epsilon(\dot\epsilon_3) = T_F(\dot\epsilon_3 + \omega_d) - T_F(\omega_d). \tag{20}$$

The discrete equivalent of the continuous model (17) with the sampling time T_s is defined as follows:

$$\boldsymbol{\epsilon}_{i+1} = \mathbf{A}_D\boldsymbol{\epsilon}_i + \mathbf{B}_D u_i^\epsilon + \mathbf{D}_D T_{F,\,i}^\epsilon, \tag{21}$$

where the matrices $\mathbf{A}_D$, $\mathbf{B}_D$, $\mathbf{D}_D$ of the discrete model are determined from the matrices $\mathbf{A}$, $\mathbf{B}$, $\mathbf{D}$ of the continuous model (17) by employing the zero-order hold method:

$$\begin{aligned}\mathbf{A}_D =& e^{\mathbf{A}T_s}, \qquad \mathbf{B}_D = \int_0^{T_s} e^{\mathbf{A}t}\,\mathrm{d}t\,\mathbf{B},\\ \mathbf{D}_D =& \int_0^{T_s} e^{\mathbf{A}t}\,\mathrm{d}t\,\mathbf{D}.\end{aligned} \tag{22}$$

The performance index for the control is defined as the quadratic function in the error space on some time horizon $S > 0$,

$$J = \sum_{i=0}^{S}\left(\boldsymbol{\epsilon}_i^T\mathbf{Q}\boldsymbol{\epsilon}_i + u_i^\epsilon R u_i^\epsilon\right). \tag{23}$$

It can be observed that the aim of the control is to minimize the errors $\boldsymbol{\epsilon}$, u^ϵ between the system state and control and their reference trajectories $\mathbf{x}_d$, u_d. The convergence of the quadratic terms of the objective to 0 means that the control successfully steers the system to the desired angular velocity ω_d.

The proposed control scheme that will be presented in Section 3 computes the control value accordingly to the direct state feedback. This form of control sets the requirement on the angular displacements and velocities along with the motor's torque to be measurable. Although this paper is concerned with the theoretical control problem and these parameters are assumed to be directly measurable, it is important to discuss possible solutions to measure state signals in practical realisation. The direct measurements of the angular displacements and velocities could be performed by the incorporation of incremental encoders into the experimental design. The torque of the assumed DC motor model is proportional to the current i induced in the circuit, and thus its value can be measured directly. If some of the aforementioned parameters cannot be directly measured, it is proposed to use a state observer, e.g., the Kalman filter, to estimate the unknown values.

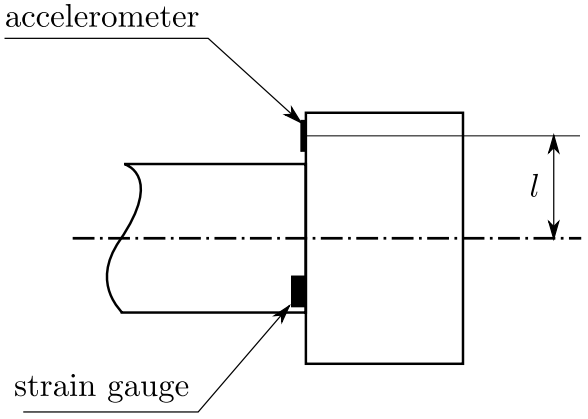

Fig. 2. Scheme of the torque measurement setting.

The estimation of the disturbance torque T_{dist} acting on the controlled object is crucial for proper work of the developed control scheme. In the presence of stick-slip oscillations, such estimation is not straightforward. Because of that, the measurement setup depicted in Fig. 2 is proposed. At some predefined distance l from the axis of rotation of the drill bit, an accelerometer is placed. The measurement of the acceleration tangent to the rotation, a, allows computing angular acceleration $\ddot{\phi}_3$ of the body:

$$\ddot{\phi}_3 = \frac{a}{l}. \tag{24}$$

In addition to the accelerometer, the strain gauge is placed at the joint of the drill string and the bit. Knowing the material properties of the machine, the torque T_B between the bit and the drill string can be easily established. For the proposed simplified model, the analogous setting is to measure the angular acceleration of the body I_3 and the torque generated by the spring k_3. The summary disturbance torque T_{dist} acting on a drill bit is then estimated according to the second law of dynamics,

$$T_{\text{dist}} = I_3\ddot{\phi}_3 - T_B. \tag{25}$$

3. Formulation of the control scheme

3.1. Optimal control problem. Using the dynamical model (21) of the system presented in Fig. 1 along with the definition of the reference trajectory (14) and the control constraints (6), the stabilization objective in the form of the optimal control problem stated in the error space $\boldsymbol{\epsilon}$ can be finally presented as follows:

Find

$$u^{\epsilon}_{i=0,1,\dots} = \arg\min J = \sum_{i=0}^{S} \left(\boldsymbol{\epsilon}_i^T \mathbf{Q} \boldsymbol{\epsilon}_i + (u_i^{\epsilon})^T \mathbf{R} u_i^{\epsilon}\right)$$

subject to

$$\begin{aligned} \boldsymbol{\epsilon}_{i+1} &= \mathbf{A}_D \boldsymbol{\epsilon}_i + \mathbf{B}_D u_i^{\epsilon} + \mathbf{D}_D T^{\epsilon}_{F,\,i}(\dot{\epsilon}_{i,\,3}), \\ \boldsymbol{\epsilon}_0 &= \mathbf{x}_d(0), \\ u_i^{\epsilon} &\in [-u_{\max} - u_d; u_{\max} - u_d], \quad i = 0, 1, \dots . \end{aligned} \tag{26}$$

Because the nonlinear function $T^{\epsilon}_{F,\,i}(\dot{\epsilon}_{i,\,3})$ that represents the friction torque is assumed to be changing over time and unknown before the beginning of the operation, it is not possible to obtain the solution to the optimal control problem (26). In order to overcome this issue, we suggest a controller that adapts the control decision to the measured values of the friction torque and gives suboptimal results with reference to the problem (26).

3.2. Suboptimal adaptive control. In this section, the adaptive suboptimal control scheme for a particular problem (26) is defined. It is worth mentioning that the proposed control scheme can be applied to any stabilization control problem for linear dynamical systems subjected to a measurable disturbance with the performance index given in the form of a quadratic function (23).

Let us now consider the problem defined in (26), neglecting the impact of the disturbance:

$$\boldsymbol{\epsilon}_{i+1} = \mathbf{A}_D \boldsymbol{\epsilon}_i + \mathbf{B}_D u_i^{\epsilon}, \quad \boldsymbol{\epsilon}_0 = -\mathbf{x}_d(0). \tag{27}$$

The control strategy minimizing the quadratic performance index for the dynamical model neglecting the disturbance (27) is known as the linear quadratic regulator and has the form of a proportional feedback control:

$$u_i^{\epsilon *} = -\mathbf{K}_i \cdot \boldsymbol{\epsilon}_i, \tag{28}$$

$$\mathbf{K}_i = \left(\mathbf{R} + \mathbf{B}_D^T \mathbf{P}_{i+1} \mathbf{B}_D\right)^{-1} \mathbf{B}_D^T \mathbf{P}_{i+1} \mathbf{A}_D, \tag{29}$$

where $\mathbf{P}_i$ is a symmetric positive definite matrix satisfying the nonlinear dynamic equation (a discrete-time Riccati dynamic equation)

$$\begin{aligned}\mathbf{P}_i =& \mathbf{Q} + \mathbf{A}_D^T\mathbf{P}_{i+1}\mathbf{A}_D \\ &- \mathbf{A}_D^T\mathbf{P}_{i+1}\mathbf{B}_D\left(\mathbf{R} + \mathbf{B}_D^T\mathbf{P}_{i+1}\mathbf{B}_D\right)^{-1} \\ &\cdot \mathbf{B}_D^T\mathbf{P}_{i+1}\mathbf{A}_D, \\ \mathbf{P}_S =& \mathbf{0}.\end{aligned} \tag{30}$$

The control law defined by (28), (29) and (30), synthesized for the incomplete system dynamics (27), will not generate the optimal control for the true system subjected to a friction torque (21). In extreme cases, such control may result in system instability.

Let us now assume that the disturbance signal $f_i = T^{\epsilon}_{F,i}(\dot{\epsilon}_{i,3})$ can be approximated by the linear time-invariant discrete dynamic system of the order n:

$$\mathbf{F}_{i+1} = \begin{bmatrix} f_{i+1} & f_i & \cdots & f_{i+2-n}\end{bmatrix}^T = \mathbf{G}\cdot\mathbf{F}_i. \tag{31}$$

The state space equation of the autonomous approximation of the original, disturbed system (21) that makes use of the disturbance model (31) can be now formulated as follows:

$$\begin{bmatrix}\boldsymbol{\epsilon}_{i+1}\\ \mathbf{F}_{i+1}\end{bmatrix} = \mathbf{A}_{\text{aut.}}\begin{bmatrix}\boldsymbol{\epsilon}_i\\ \mathbf{F}_i\end{bmatrix} + \mathbf{B}_{\text{aut.}}u_i^{\epsilon}, \tag{32}$$

$$\mathbf{A}_{\text{aut.}} = \begin{bmatrix}\mathbf{A}_D & \begin{bmatrix}\mathbf{D}_D & \mathbf{0} & \cdots & \mathbf{0}\end{bmatrix}\\ \mathbf{0} & \mathbf{G}\end{bmatrix},$$

$$\mathbf{B}_{\text{aut.}} = \begin{bmatrix}\mathbf{B}_D\\ \mathbf{0}\end{bmatrix}.$$

Let us also redefine the matrix $\mathbf{Q}$ such that it accommodates the augmented state vector

$$\mathbf{Q}_{\text{aut.}} = \begin{bmatrix}\mathbf{Q} & \mathbf{0}\\ \mathbf{0} & \mathbf{0}\end{bmatrix}. \tag{33}$$

For the system (32) defined by the matrices $\mathbf{A}_{\text{aut.}}$, $\mathbf{B}_{\text{aut.}}$, and the control objective defined by $\mathbf{Q}_{\text{aut.}}$ and $\mathbf{R}$, the linear quadratic regulator on a finite horizon can be synthesized as in (28)–(30).

The control generated by the adaptive control method is discrete and within the i-th loop of the algorithm takes the form

$$u_i^{\epsilon} = -\mathbf{K}_0\begin{bmatrix}\boldsymbol{\epsilon}_i\\ \mathbf{F}_i\end{bmatrix}, \tag{34}$$

where $\boldsymbol{\epsilon}_i$ is the measured state of the structure consisting of angular deflections and velocities of all four bodies and the torque induced by the motor, while the vector $\mathbf{F}_i$ denotes the last n measured values of the disturbance.

It is important to point out that the control value adapts to the measured disturbance not only by means of the direct feedback but also by the adjustment of the value of the feedback matrix $\mathbf{K}_0$ in accordance with the currently established disturbance model (31). The quality of this control strategy clearly depends on the quality of the approximation of the disturbance.

In the present paper, the discrete dynamics of the disturbance are modeled as an autoregressive (AR) model. An example of using autoregressive modeling in traffic control is presented by Pisarski and Canudas-de-Wit (2016). Let

$$\begin{bmatrix} f_i & f_{i+1} & \cdots & f_{i+N-1}\end{bmatrix} \tag{35}$$

be the time series of the disturbance f_i sampled with the same period as the discretization period T_s in (21). The length of the series is N. To obtain this vector, one can use measurements of the past N values of the disturbance or employ an external signal extrapolator which provides forecasts of the future values of the disturbance. The design of such an extrapolator does not fall within the scope of this paper, and it is assumed that the disturbance approximation is based on the past values of the perturbation.

The deterministic autoregressive model of order n has the following form:

$$f_i = \sum_{j=1}^{n}\theta_j f_{i-j} = \begin{bmatrix} f_{i-1} & f_{i-2} & \cdots f_{i-n}\end{bmatrix}\cdot\begin{bmatrix}\theta_1\\ \theta_2\\ \vdots\\ \theta_n\end{bmatrix}. \tag{36}$$

To fit the autoregressive model to the provided signal values in the least-squares sense, the vector of weights $\boldsymbol{\Theta} = \begin{bmatrix}\theta_1 & \theta_2 & \cdots & \theta_n\end{bmatrix}^T$ should then be computed by

$$\boldsymbol{\Theta} = \mathbf{H}^{+}\begin{bmatrix}f_{i+n}\\ f_{i+n+1}\\ \vdots\\ f_{i+N-1}\end{bmatrix}, \tag{37}$$

where $\mathbf{H}^{+}$ denotes the Penrose inverse matrix of the matrix $\mathbf{H}$:

$$\mathbf{H} = \begin{bmatrix} f_{i+n-1} & \cdots & f_i\\ f_{i+n} & \cdots & f_{i+1}\\ \vdots & \ddots & \vdots\\ f_{i+N-2} & \cdots & f_{i+N-n-1}\end{bmatrix}. \tag{38}$$

It is easy to conclude that the number of the values (the size of the signal window) N considered and the order of the model n have to satisfy the inequality

$$N \geq n+1. \tag{39}$$

The model (36) can be reformulated in the discrete state-space representation

$$\begin{bmatrix} f_{i+1} \\ f_i \\ \vdots \\ f_{i-n+2} \end{bmatrix} = \begin{bmatrix} \theta_1 & \theta_2 & \cdots & \theta_{n-1} & \theta_n \\ 1 & 0 & \cdots & 0 & 0 \\ 0 & 1 & \ddots & 0 & 0 \\ \vdots & \ddots & \ddots & \ddots & \vdots \\ 0 & 0 & \cdots & 1 & 0 \end{bmatrix} \cdot \begin{bmatrix} f_i \\ f_{i-1} \\ \vdots \\ f_{i-n+1} \end{bmatrix}. \tag{40}$$

The model (40) can be directly applied to (32) and the control strategy (34) can be calculated.

To attain a high accuracy of the control strategy, this model approximation is calculated periodically with the same period T_s as the time discretization of the system and the period of the disturbance time series. Since the new calculation of the model (40) changes the system dynamics (32), the calculation of the control law also has to be conducted.

If the approximation of the disturbance is based on the preceding values of the signal, it is obvious that the control scheme cannot be initiated until the number of the available past values of the disturbance is not less than some set parameter $N_{\min}$ ($N_{\min} \leq N$). It is clear that $N_{\min}$ should be greater than the order of approximation n. If the dynamic equation governing the evolution of the disturbance $f(t)$ in time is nonlinear and/or varies in time, it is highly recommended to choose relatively small values of N and $N_{\min}$. Otherwise, the past measurements that correspond to the previous character of the disturbance will dominate the measurement vector (35) over the new measurements. Because the approximation of the disturbance calculated by Eqn. (37) depends on the whole measurement vector, it would be biased towards the outdated character of the load. It is important to observe that the measurements that reflect the former behaviour of the load will still appear in the measurement vector until the next N values of the disturbance are measured.

It must be emphasized that in some cases the dynamics of the disturbance have a lower order than the set order of the approximation n. In such a case, the coefficients of the autoregressive approximation can erratically alter the response to small changes in the data. Such a phenomenon is known as multicollinearity (for the review of the detection methods of the multicollinearity phenomenon, see the works of Farrar and Glauber (1967) or Alin (2010)). The excessive sensitivity of the model to the provided data can result in instability of the synthesized control law, e.g., spikes of high magnitude of the control value. This situation can be avoided if the order n of the autoregressive model is adapted to the unusual disturbance. The reduction of the order n can be made dependent on the value of the condition number of the rectangular matrix $\mathbf{H}$ (see Farrar and Glauber, 1967): if this number is large, e.g., greater than some set number λ, the order n should be reduced. The number λ is defined arbitrarily according to the experience of the controller designer. In real life applications of the proposed control method, the measurement noise acts against multicollinearity, so the implementation of the procedure described above should be considered for each individual control problem case.

Algorithm 1. Initialization.

1: Set the discretization period T_s.
2: Set the order of the model approximation n.
3: Set the size of the signal window N and minimal size $N_{\min}$.

Require: $N \geq n+1$.

4: Set the horizon of the LQR control $T_{\text{horizon}} = S \cdot T_s$ (S as in (26)).
5: Set the matrices $\mathbf{Q}$ and $\mathbf{R}$.
6: Compute the discrete equivalent (21) of the system (17) for the time period T_s.

Algorithm 2. Main loop.

1: **if** the number of available measurements of the disturbance $l \geq N_{\min}$ **then**
2: Measure the state of the system $\boldsymbol{\epsilon}_i$ and value of the disturbance f_i.
3: Compute the vector of AR weights $\boldsymbol{\Theta}$ using Eqn. (37).
4: Use $\boldsymbol{\Theta}$ to generate $\mathbf{G}$ as in (40).
5: Synthesize the model (32) using the matrices $\mathbf{A}_D$, $\mathbf{B}_D$, $\mathbf{D}_D$, calculated at the initialization, and $\mathbf{G}$.
6: Calculate $\mathbf{P}_1$ back in time according to (30).
7: Calculate $\mathbf{K}_0$ according to (29).
8: Set the control value $\mathbf{u}_i = u_i^{\epsilon} = -\mathbf{K}_0 \begin{bmatrix} \boldsymbol{\epsilon}_i \\ \mathbf{F}_i \end{bmatrix}$ (see (34)).
9: **end if**

The initialization of the controller is presented in Algorithm 1. This procedure is executed once at the beginning of the control. The main loop of the adaptive scheme is presented in Algorithm 2. This loop is executed within time period T_s.

4. Numerical results

In this section, the numerical results are presented. The performance of the proposed control scheme is compared with the results established by the linear-quadratic-Gaussian (LQG) regulator.

The framework of the linear-quadratic-Gaussian controller employs a specific form of the dynamical equations of the system dynamics. It is assumed that, in general, not all states of the system can be measured by the sensors and that two types Gaussian noise act on the system: measurement noise w, replicating the errors

Algorithm 3. LQG control loop.

1: Measure the output of the system $\mathbf{y}_k = \boldsymbol{\epsilon}_k$ according to Eqn. (41).
2: Update state estimation: $\hat{\mathbf{x}}_k = \mathbf{A}\hat{\mathbf{x}}_{k-1} + \mathbf{B}u_{k-1} + \mathbf{S}_{\text{LQG}}\left(\mathbf{y}_k - \mathbf{L}\left[\mathbf{A}\hat{\mathbf{x}}_{k-1} + \mathbf{B}u_{k-1}\right]\right)$.
3: Update control: $u_k = -\mathbf{K}_{\text{LQG}}\hat{\mathbf{x}}_k$.

of the sensors, and system noise v corresponding to the disturbances affecting the system. The dynamical model (21) adopted for the LQG framework is of the form

$$\begin{aligned} \boldsymbol{\epsilon}_{i+1} &= \mathbf{A}_D\boldsymbol{\epsilon}_i + \mathbf{B}_D u_i^{\epsilon} + \mathbf{D}_D v, \\ \mathbf{y}_i &= \mathbf{L}\boldsymbol{\epsilon}_i + \mathbf{w}, \end{aligned} \tag{41}$$

where $\mathbf{y}$ is the measured output vector, $\mathbf{L}$ is the output matrix, v is the Gaussian system noise with variance V, and $\mathbf{w}$ is the Gaussian measurement noise with covariance matrix $\mathbf{W}$.

The LQG regulator feedback matrix $\mathbf{K}_{\text{LQG}}$ and the Kalman filter matrix $\mathbf{S}_{\text{LQG}}$ are calculated as follows:

$$\begin{aligned} \mathbf{K}_{\text{LQG}} &= \left(\mathbf{R} + \mathbf{B}^T\mathbf{P}_{\text{LQG}}\mathbf{B}\right)^{-1}\mathbf{B}\mathbf{P}_{\text{LQG}}\mathbf{A}, \\ \mathbf{S}_{\text{LQG}} &= \boldsymbol{\Sigma}_{\text{LQG}}\mathbf{L}^T\left(V + \mathbf{L}\boldsymbol{\Sigma}_{\text{LQG}}\mathbf{L}^T\right)^{-1}, \end{aligned} \tag{42}$$

where $\mathbf{P}_{\text{LQG}}$, $\boldsymbol{\Sigma}_{\text{LQG}}$ are the solutions of the respective algebraic Riccati equations,

$$\begin{aligned} \mathbf{P}_{\text{LQG}} &= \mathbf{A}^T\mathbf{P}_{\text{LQG}}\mathbf{A} - \left(\mathbf{A}^T\mathbf{P}_{\text{LQG}}\mathbf{B}\right) \\ &\quad \cdot \left(\mathbf{R} + \mathbf{B}^T\mathbf{P}_{\text{LQG}}\mathbf{B}\right)^{-1}\left(\mathbf{B}^T\mathbf{P}_{\text{LQG}}\mathbf{A}\right) + \mathbf{Q}. \\ \boldsymbol{\Sigma}_{\text{LQG}} &= \mathbf{A}\boldsymbol{\Sigma}_{\text{LQG}}\mathbf{A}^T - \left(\mathbf{A}\boldsymbol{\Sigma}_{\text{LQG}}\mathbf{L}^T\right) \\ &\quad \cdot \left(V + \mathbf{L}\boldsymbol{\Sigma}_{\text{LQG}}\mathbf{L}^T\right)^{-1}\left(\mathbf{L}\boldsymbol{\Sigma}_{\text{LQG}}\mathbf{A}^T\right) + \mathbf{W}. \end{aligned} \tag{43}$$

The matrices $\mathbf{K}_{\text{LQG}}$ and $\mathbf{P}_{\text{LQG}}$ are calculated by employing the same matrices $\mathbf{Q}$ and R as the feedback law of the adaptive scheme in (46). The LQG regulator operates in the infinite loop defined in Algorithm 3.

Both the proposed control scheme defined in Algorithm 2 and the LQG regulator were tested for the angular velocity stabilization problem with friction models of the form (1) and different parameters depicted in Tables 2–4. The torque–angular velocity characteristics of each used friction model are depicted in respective sections concerning particular disturbance scenario. In addition, in Section 4.5 a spectral analysis of the control system considered is conducted, and in Sections 4.6 and 4.7 the dependence of the performance of the proposed scheme on various model and algorithm parameters is studied.

The performance of the adaptive and LQG controllers is compared through the computation of the quadratic cost function

$$J_x(t) = \int_0^t \boldsymbol{\epsilon}^T(s)\mathbf{Q}\boldsymbol{\epsilon}(s)\,\mathrm{d}s. \tag{44}$$

Because the ultimate goal of the control is to steer the system to the reference trajectory $\mathbf{x}_d$ despite the control expenditure, the function (44) does depend only on the error of the state of the system. The time horizon t varies for every simulation case and is equal to the simulation duration.

The analogous performance criterion for the error of the control u_ϵ is not considered a proper measurement of the performance in the simulations, because it does not reflect the goal of the control. As a motivational example, let us observe that the for the constant control $u_\epsilon = 0$ such a criterion $\int_0^t u_\epsilon(s)Ru_\epsilon(s)\,\mathrm{d}s$ will be equal to 0; however, the trajectory of the system considered will diverge as a result of the self-induced oscillations.

The assessment of the control input performance is rather conducted by measurement of the energy used by the motor on the entire simulation interval,

$$E_u = \int_0^t \frac{u^2(s)}{R_{DC}}\,\mathrm{d}s. \tag{45}$$

The mechanical parameters of the system considered, as well as both the proposed adaptive and LQG controller settings are listed below. The values of the parameters of the studied drilling machine model (4) employed in the computations are summarized in Table 1.

Table 1. Values of the system parameters.

Parameter	Value
R_{DC}	$0.472\,\Omega$
L	$7.85\,\mathrm{mH}$
K_e	$4.9\,\mathrm{N\,m\,A^{-1}}$
I_0	$5.56 \cdot 10^{-2}\,\mathrm{kg\,m^2}$
I_{1-2}	$1 \cdot 10^{-1}\,\mathrm{kg\,m^2}$
I_3	$1.2114\,\mathrm{kg\,m^2}$
k_{1-3}	$200\,\mathrm{N\,m\,rad^{-1}}$
c_{1-3}	$1\,\mathrm{N\,m\,s\,rad^{-1}}$

For every simulation case it is assumed that the constraint of the input defined in (6) is $u_{\max} = 200$ V.

For the objective function (23), we assume

$$R = 10^{-4}, \quad \mathbf{Q} = \begin{bmatrix} \mathbb{I}_8 & \mathbf{0} \\ \mathbf{0} & 0 \end{bmatrix}. \tag{46}$$

The above form of the matrix $\mathbf{Q}$ results from the fact that the goal of the control is to minimize only the error of the states representing the angle and angular velocity

Table 2. Values of the friction parameters for the first scenario.

Parameter	Value
T_{C1}	$60\,\mathrm{N\,m}$
T_{B1}	$190\,\mathrm{N\,m}$
c_{v1}	$0.05\,\mathrm{s\,rad^{-1}}$
f_{T1}	$0.001\,\mathrm{N\,m\,s\,rad^{-1}}$
$\dot{\phi}_{c1}$	$0.0001\,\mathrm{rad\,s^{-1}}$

deflection of the system. Such a value of R was used to meet value constrains on the input defined in (6).

The order of the approximating autoregressive model of the adaptive control method was set to $n = 3$. The size of the window was set to $N = 220$. The minimal size of the window was $N_{\min} = 40$, and the sample time chosen for the simulation was $T_s = 0.005\,\mathrm{s}$. It can be emphasized that the time of execution of one call of the proposed control scheme for this system on a PC-class computer is approximately equal to $T_e \approx 0.000259\,\mathrm{s}$, so the devised control method fulfills the requirements for real-time computing.

For the control system described in this paper, it is assumed that the output matrix of the LQG regulator in Eqn. (41) is equal to $\mathbf{L} = \mathbb{I}_9$, i.e., the measurements of all states x are available. The LQG regulator was synthesized for various values of V and $\mathbf{W}$ and tested for the simulation scenario described in Section 4.1. The final values of these parameters were then chosen such that the performance index obtained in the control simulation was minimal, and they are as follows:

$$V = 1, \quad \mathbf{W} = 5.5 \cdot \mathbb{I}_9. \tag{47}$$

Such a strategy was used to assure that the potential improvement of the adaptive scheme in comparison to the LQG control is not caused by a poor choice of the LQG parameters.

4.1. Case with single friction. In the first simulation, the goal of the controller is to steer the object from the initial state (10) to the reference trajectory (14) with the setpoint angular velocity $\omega_s = 10\,\mathrm{rad\,s^{-1}}$. The time of the simulation was set to $T = 8\,\mathrm{s}$. The values of the friction parameters are given in Table 2. The characteristics of the friction torque are depicted in Fig. 3. For the first simulation scenario, it is assumed that the disturbance torque consists of a friction torque only. The impact of random noise on the quality of control is analyzed in Section 4.2. The results of the simulation are compared with those of the LQG control in Figs. 4 and 5.

As one can see, the control generated by the developed control method brings the system to the reference trajectory in about two seconds (Fig. 5). Then the objective function (44) depicted in Fig. 4 stabilizes. This means that all the displacements of the angles and angular velocities of the bodies from the reference trajectory $\mathbf{x}_d$ approach zero. On the other hand, the LQG control results in a greater final value of the objective function. The performance objective (44) equals 91.73 for the proposed control scheme and 105.5 for the LQG control; the improvement is $13\,\%$.

The total energy consumed by the system for the LQG control is $E_u \approx 83000$ J, whereas the adaptive control scheme resulted in $E_u \approx 88000$ J. This 6% increase of energy utilisation is a result of the sharp peaks of the control at the beginning of the simulation (see Fig. 4 (b)).

The LQG control provides greater absolute values of the system errors, which can be seen in Fig. 5. These simulation results prove the ability of the developed adaptive method to control the system under external disturbances with higher quality than in the case of the LQG control.

4.2. Case with single friction characteristics with noise. In this section, the ability of the control of the system in the presence of Gaussian noise is tested. The parameters of the system and the proposed control algorithm are the same as in the previous section. Uniform signal noise with variance g and mean 0 is added to the friction model from the previous section. The simulation time was set to $T = 8\,\mathrm{s}$. The resulting variation in the friction force over time for the two studied variances $g = 1\,\mathrm{N^2\,m^2}$ and $g = 200\,\mathrm{N^2\,m^2}$ is depicted in Fig. 7.

A comparison of the objective function for different values of g is presented in Fig. 6. The objective function obtained at the time $8\,\mathrm{s}$ of the simulation increases with an increase in the variance g. Figure 8(a) shows that the value of the objective function increases in time. In fact, when $g \neq 0$, the objective function obviously diverges. However, even for a noise variance as high as $g = 200\,\mathrm{N^2\,m^2}$, Fig. 9 shows that the values of the errors are bounded and have lower values than for the

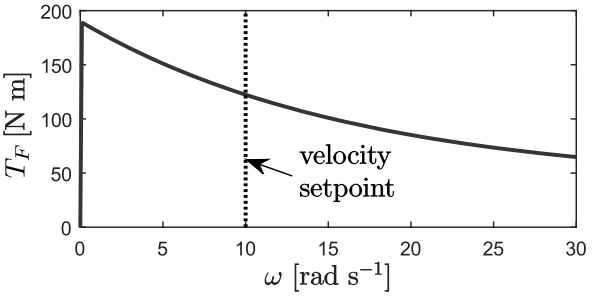

Fig. 3. Torque–angular velocity characteristics of the friction torque model assumed for the first simulation scenario.

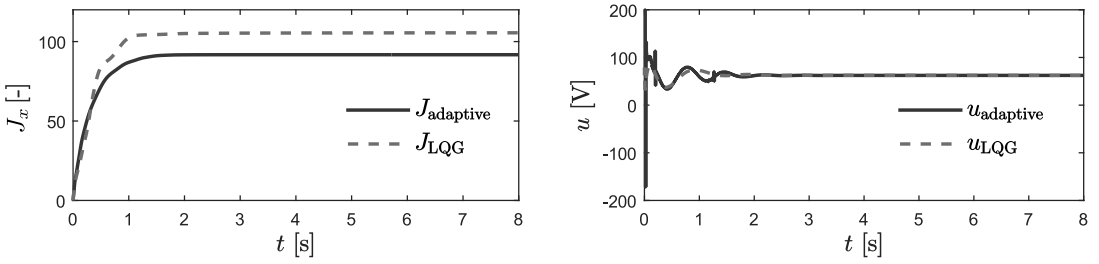

(a) (b)

Fig. 4. Comparison of the numerical simulation of the adaptive controller of Algorithm 2 and the LQG regulator of Algorithm 3 in the first scenario: objective function values obtained by the proposed scheme and the LQG regulator (a), control values generated by the adaptive controller and the LQG regulator (b).

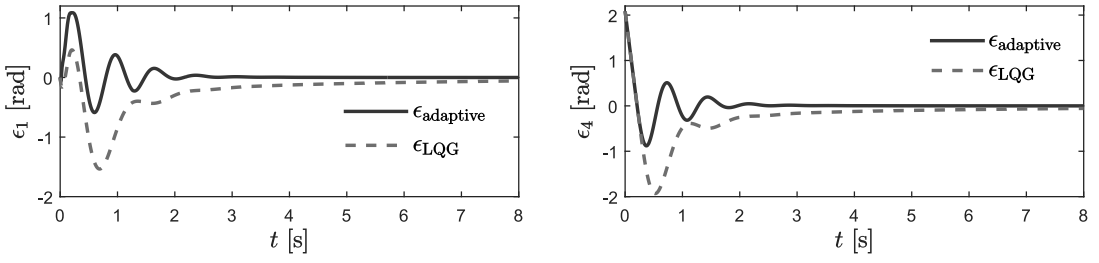

(a) (b)

Fig. 5. Comparison of the numerical simulation of the adaptive controller of Algorithm 2 and the LQG regulator of Algorithm 3 in the first scenario: error of the angular displacement of the first mass controlled with the proposed algorithm and LQG control (a), error of the angular displacement of the fourth mass controlled with the proposed algorithm and LQG control (b).

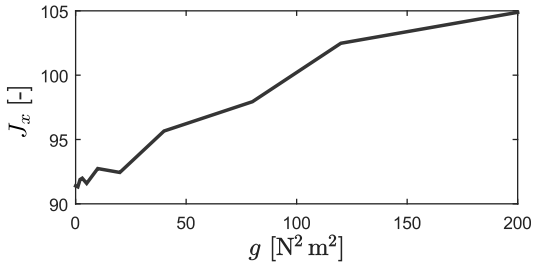

Fig. 6. Objective function J_x achieved at the simulation time $t = 8\,\mathrm{s}$ for different variances of the noise g.

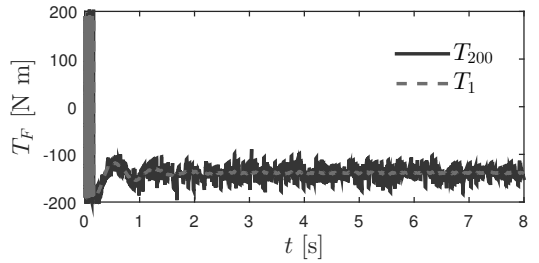

Fig. 7. Friction torque values in the simulation for the noise variance $g = 1\,\mathrm{N}^2\,\mathrm{m}^2$ and $g = 200\,\mathrm{N}^2\,\mathrm{m}^2$. T_{200} stands for the friction torque generated in the simulation with noise variance $g = 200\,\mathrm{N}^2\,\mathrm{m}^2$ and T_1 stands for the simulation with $g = 1\,\mathrm{N}^2\,\mathrm{m}^2$.

LQG control without noise, as depicted in Fig. 4. For $g = 1\,\mathrm{N}^2\,\mathrm{m}^2$, the value of the objective function is 91.3 and for $g = 200\,\mathrm{N}^2\,\mathrm{m}^2$ J_x it is equal to 101.3.

4.3. Case with varying friction characteristics. In this section, the scenario with a step change in the friction characteristic is studied. As in the previous case, the results are compared with the LQG control. The initial point and the angular velocity set point are the same as in the previous cases. In the first phase of the simulation, for $t \in [0\,\mathrm{s}, 1\,\mathrm{s})$, the friction torque has the parameters assumed as in the first column of Table 3 and at the time $t = 1\,\mathrm{s}$, the parameters of the friction change to the second set of parameters, presented in the second column of Table 3. The simulation runs then until the final time $T = 9\,\mathrm{s}$. Both the torque characteristics defined by the parameters in Table 3 are presented in Fig. 10. The sets of parameters were chosen to provide an unchanged friction torque value for ω_d. This property of the friction was chosen to avoid a sudden jump of the constant in the formula (18). It can be observed that the friction characteristics significantly change at the time $1\,\mathrm{s}$.

The results are depicted in Figs. 11 and 12. The curves depict the results for the LQG control method (dashed lines) and are compared with our adaptive control method (solid lines). In the first interval of the simulation

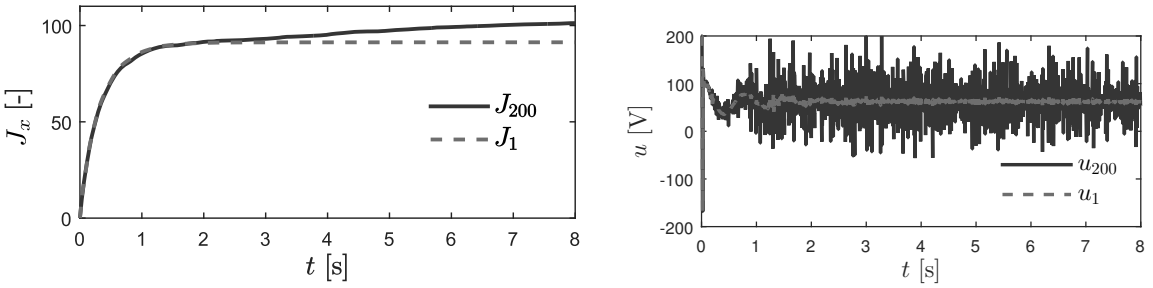

(a) (b)

Fig. 8. Comparison of the numerical simulation of the adaptive scheme of Algorithm 2 for the friction noise gain $g = 1\,\mathrm{N}^2\,\mathrm{m}^2$ and $g = 200\,\mathrm{N}^2\,\mathrm{m}^2$: objective functions achieved with the control scheme (J_{200} stands for the result of simulation governed with noise variance $g = 200\,\mathrm{N}^2\,\mathrm{m}^2$ and J_1 stands for the trajectory of simulation with the noise variance $g = 1\,\mathrm{N}^2\,\mathrm{m}^2$) (a), control values generated by Algorithm 2 (b).

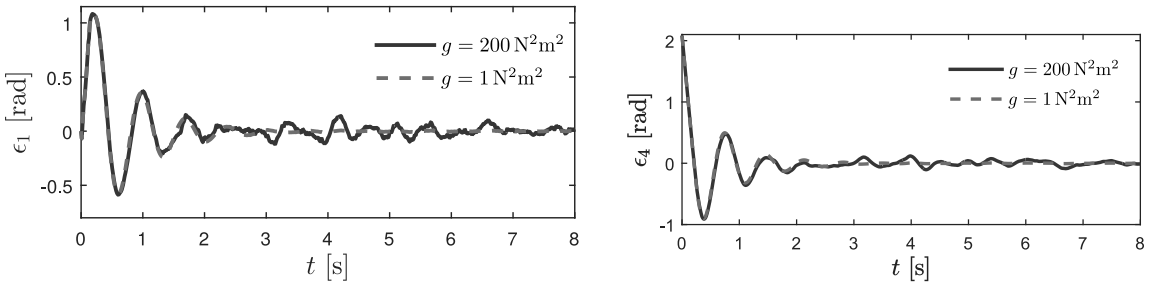

(a) (b)

Fig. 9. Comparison of the numerical simulation of the control scheme of Algorithm 2 for the friction noise gain $g = 1\,\mathrm{N}^2\,\mathrm{m}^2$ and $g = 200\,\mathrm{N}^2\,\mathrm{m}^2$: error of the angular displacement of the first body (a), error of the angular displacement of the fourth body (b).

Table 3. Values of the friction parameters for the second scenario.

Parameter	First stage	Second stage
T_{C2}	$200\,\mathrm{N\,m}$	$45\,\mathrm{N\,m}$
T_{B2}	$210\,\mathrm{N\,m}$	$310.5518\,\mathrm{N\,m}$
c_{v2}	$0.05\,\mathrm{s\,rad}^{-1}$	$0.05\,\mathrm{s\,rad}^{-1}$
f_{T2}	$0.001\,\mathrm{N\,m\,s\,rad}^{-1}$	$0.001\,\mathrm{N\,m\,s\,rad}^{-1}$
$\dot{\phi}_{c2}$	$0.0001\,\mathrm{rad\,s}^{-1}$	$0.0001\,\mathrm{rad\,s}^{-1}$

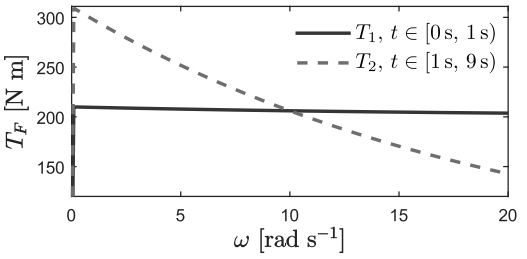

Fig. 10. Friction torque vs. angular velocity characteristics for the second simulation scenario. T_1: characteristics of the friction torque at the first stage of the simulation, $t \in [0\,\mathrm{s}, 1\,\mathrm{s})$, T_2: characteristics of the friction torque in the second stage of the simulation, $t \in [1\,\mathrm{s}, 9\,\mathrm{s})$.

$t \in [0\,\mathrm{s}; 1\,\mathrm{s})$ both the adaptive scheme and the LQG regulator are stabilizing the system. In fact, the results obtained for the LQG control in the first interval are better than those for the proposed control method. The initial peak of the error of the angular displacement for the first and the fourth masses is nearly 40% greater for the system controlled by the adaptive scheme than for the LQG. This is due to the fact that the number of the measurements of the friction is small at the beginning of the simulation and the friction at this time is in the sticking phase. The generated AR model in such a case cannot be precise enough. Nevertheless, the objective functions (Fig. 11(a)) achieved in the first interval by both control algorithms have similar values. In the second stage of the simulation $t \in [1; 9]\,\mathrm{s}$, when the friction characteristics are changed, the LQG control destabilizes the system. The error trajectories (Fig. 12) for the LQG control exhibit undamped oscillations and the objective function does not converge.

The peak-to-peak amplitude of the angular displacement error of the first and the fourth body stabilizes at $0.4\,\mathrm{rad}$ and $0.7\,\mathrm{rad}$, respectively. For comparison, the proposed control method quickly achieves the goal of the control: in 1.5 seconds after the

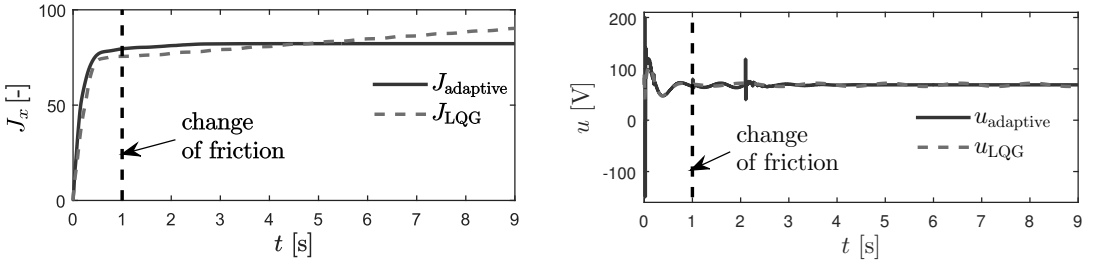

(a) (b)

Fig. 11. Comparison of the numerical results of the simulation of the adaptive controller of Algorithm 2 and the LQG regulator of Algorithm 3 in the second scenario: objective functions achieved by the control scheme and the LQG regulator (a), control values generated by the adaptive controller and the LQG regulator (b).

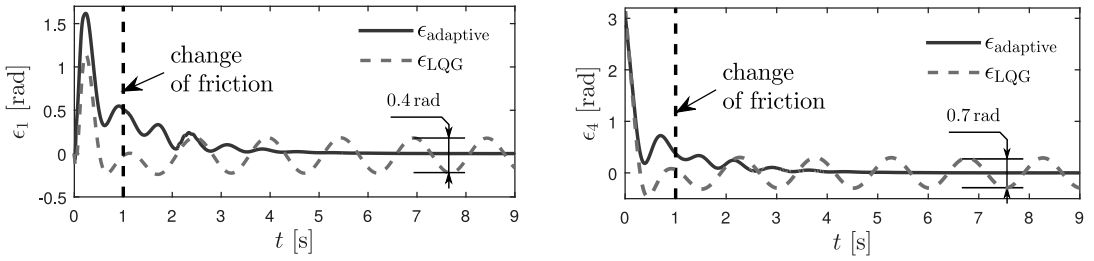

(a) (b)

Fig. 12. Comparison of the numerical results of the simulation of the adaptive controller of Algorithm 2 and the LQG regulator of Algorithm 3 in the second scenario: error of the angular displacement of the first mass controlled with the proposed control scheme and LQG control (a), error of the angular displacement of the fourth mass controlled with the proposed control scheme and LQG control (b).

friction change the adaptive scheme generates a smaller oscillation of the angular displacement than the LQG regulator, and after approximately 3 s the error trajectories of the system converge to zero. The final value of the objective function J_x obtained in simulation is 82.25, while that for the LQG control is $J = 90.28$. The results of this simulation prove the efficiency of adaptation by the proposed algorithm to a sudden change of the disturbance.

The ultimate energy consumed by the adaptive and the LQG scheme is approximately equal to 95300 J and 93400 J, respectively. The small power increase (approximately 2%) for the adaptive scheme is caused mainly by the sharp peaks of the control. What is important, the system after $t = 2\,\text{s}$ has approximately the same energy consumption for both control algorithms but the LQG control fails to stabilize the system.

As can be noticed from Fig. 11(b), the adaptive scheme yields two sharp peaks of the control at $t = 1\,\text{s}$ and $t = 2.1\,\text{s}$. The first peak is observed at $1.05\,\text{s}$, right after the step change in the friction characteristics. Because of the step change in the disturbance parameters, the time instant $t = 1\,\text{s}$ marks not only the discontinuity of the friction signal, but also the change in the signal parameters such as amplitude and frequency. Because of that, the feedback vector of the measured disturbance $\mathbf{F}_i$ is sharply changed. In addition, the change in the AR model caused by the introduction of new friction parameters results in a significantly different value of the feedback matrix $\mathbf{K}_0$. The observed peak in the control signal is a result of both aforementioned events.

In order to explain the second aberration, it is crucial to observe that the assumed disturbance measurement window $N = 220$ corresponds to the measurements interval $N \cdot T_s = 1.1\,\text{s}$. For the time interval $t \in [1,\, 2.1)$, the AR model adjusts its parameters based on the measurements corresponding to both friction models with a gradual increase in the measurements of the second one. The instant $2.1\,\text{s}$ marks the complete removal in the initial friction values from the measurement window. This event again triggers the change in the AR model parameters and, as a consequence, the change in the matrix $\mathbf{K}_0$, which explains the second peak.

It is important to emphasize that the presented simulation assumes a rather extreme scenario of the friction change, which is sudden and discontinuous. In practice, the friction character changes more smoothly. It has been validated that for such cases the control peak does not occur.

4.4. Case with two friction characteristics. In this scenario, an additional friction torque $T_2(\omega)$ applied to the

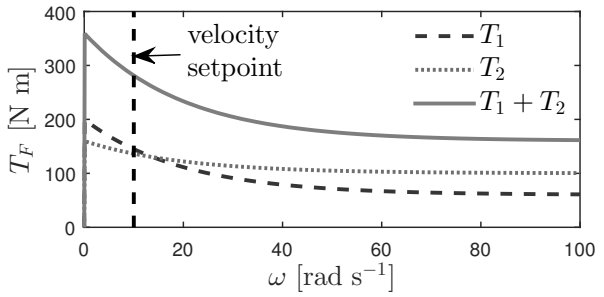

Fig. 13. Friction torque–angular velocity characteristics for the third simulation scenario.

Table 4. Values of the friction parameters for the third scenario.

Parameter	T_1	T_2
T_{C3}	$60\,\mathrm{N\,m}$	$100\,\mathrm{N\,m}$
T_{B3}	$200\,\mathrm{N\,m}$	$160\,\mathrm{N\,m}$
c_{v3}	$0.05\,\mathrm{s\,rad^{-1}}$	$0.05\,\mathrm{s\,rad^{-1}}$
f_{T3}	$0.001\,\mathrm{N\,m\,s\,rad^{-1}}$	$0.001\,\mathrm{N\,m\,s\,rad^{-1}}$
$\dot{\phi}_{c3}$	$0.0001\,\mathrm{rad\,s^{-1}}$	$0.0001\,\mathrm{rad\,s^{-1}}$

third body of the system is considered. The torque $T_1(\omega)$ is applied to the fourth body, as in the previous scenarios. The equation of motion (4) is now modified and it includes the additional friction

$$\dot{\mathbf{x}} = \mathbf{A}\mathbf{x} + \mathbf{B}u + \mathbf{D_2}\begin{bmatrix} T_2(\dot{\phi}_2) \\ T_1(\dot{\phi}_3) \end{bmatrix}, \tag{48}$$

$$\mathbf{D_2} = \begin{bmatrix} 0 & \cdots & 0 & -\frac{1}{I_2} & 0 & 0 & 0 \\ 0 & \cdots & 0 & 0 & 0 & -\frac{1}{I_3} & 0 \end{bmatrix}^T. \tag{49}$$

The steady state angular displacements between the bodies that appear in the equation of the reference trajectory (15) are as follows:

$$\begin{aligned} \xi_1 &= -\left(T_1(\omega_d) + T_2(\omega_d)\right)\frac{1}{k_1}, \\ \xi_2 &= -\left(T_1(\omega_d) + T_2(\omega_d)\right)\frac{k_1+k_2}{k_1k_2}, \\ \xi_3 &= -T_1(\omega_d)\frac{k_1k_2 + k_2k_3 + k_3k_1}{k_1k_2k_3} \\ &\quad - T_2(\omega_d)\frac{k_1+k_2}{k_1k_2}. \end{aligned} \tag{50}$$

The setpoint angular velocity has the value $\omega_d = 10\,\mathrm{rad\,s^{-1}}$.

The algorithm is now modified to take into account the simultaneously measured friction torques, both T_1 and T_2. Two dynamic models are generated by the algorithm, one for each friction function, T_1 and T_2, given in Fig. 13. The respective parameters that are used in both formulas are listed in Table 4. Figures 14 and 15 depict the results of the simulation.

Figure 14(a) shows the objective function in time. In the first second, it increases and reaches a constant value of 96.04. This means that the dynamical system is successfully steered to the reference trajectory. In the remaining period it is practically constant. The control function $u(t)$ is depicted in Fig. 14(b). It varies significantly at the beginning of the process, then slightly improves the solution, and starting from $t = 2.5\,\mathrm{s}$ remains constant. The errors ϵ_1 and ϵ_4 of the angular displacements of the first and fourth masses are presented in Fig. 15. One can notice that the errors reduce to zero rapidly. The error ϵ_1 increases from zero to the value $2.4\,\mathrm{rad}$ at the beginning and then decreases. The reason for this is that the reference angular displacement to be tracked by the system is a linear function of time, i.e., $\phi_1^d = \omega_d t$, as in (11). At the beginning of the simulation all bodies are still, while the angular error $\epsilon_1 = \phi_1^d - \dot{\phi}_1$ is increasing. This error reaches its peak at approximately $t = 0.8\,\mathrm{s}$, when the velocity of the first body $\dot{\phi}_1$ reaches the velocity setpoint ω_d. After that the error decreases and converges to zero.

The results of this simulation are similar to those achieved for the first simulation scenario. The derived control scheme effectively steers the system to the desired trajectory. A comparison with the results of the first scenario suggests that the proposed control method can be applied to complex disturbance configurations, such as two disturbances of different characteristics applied to the system.

4.5. Spectral analysis. To adequately verify the adaptive controller's ability to counteract a load of wide-range frequency, a spectral analysis of the control system was conducted. The dynamical model (4) governed by the proposed control scheme defined in Section 3 has been subjected to a sinusoidal disturbance with the frequency from the range $f \in [0.1, 20]$ Hz. The steady-state amplitudes of the dynamical system's state $\mathbf{x}$ were then measured.

In this simulation scenario, the goal of the control is to steer the system to the origin and, as a result, the algorithm can be formulated directly for the state-space formulation (4) rather than the error–space (17). The parameters of the algorithm remain the same as for the previous scenarios, i.e., $n = 3$, $N = 220$, $N_{\min} = 40$ and $T_s = 0.005\,\mathrm{s}$, with $\mathbf{Q}$, R defined as in (46).

The amplitude spectra obtained with the adaptive control scheme were compared with the results of the same analysis conducted for the LQG regulator. The values of the correlation matrices $\mathbf{W}$ and V remain the same as in the previous simulations.

The results of the analysis are presented in Figs. 16 and 17, which depict amplitude spectra of the angular deflections and velocities of the bodies I_1 and I_3. It can be observed that the proposed scheme results in a

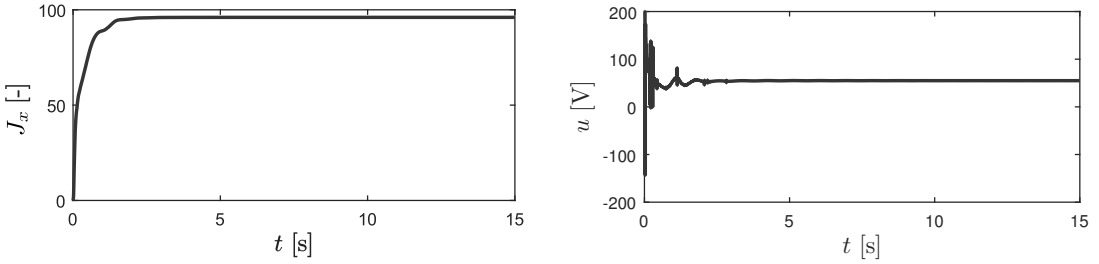

(a) (b)

Fig. 14. Results of the numerical simulation of the proposed control scheme of Algorithm 2: objective functions achieved by the scheme (a), control values generated by the scheme (b).

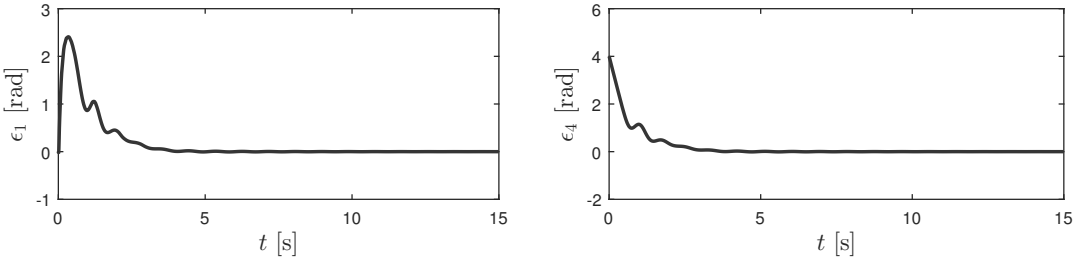

(a) (b)

Fig. 15. Results of the numerical simulation of the proposed control scheme of Algorithm 2: error of the angular displacement of the first mass under algorithm control (a), error of the angular displacement of the fourth mass under algorithm control (b).

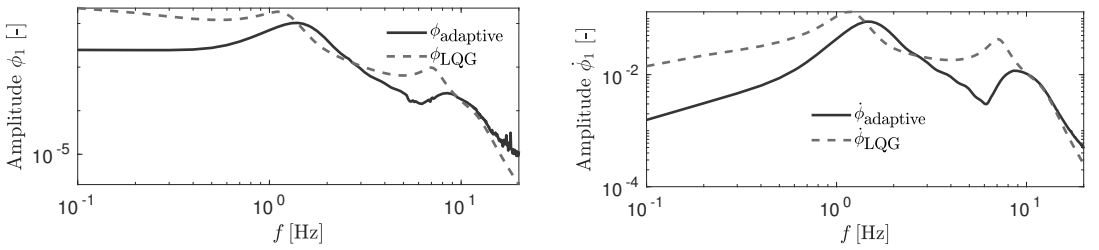

(a) (b)

Fig. 16. Amplitude spectra of the angular deflection ϕ_1 (a) and the angular velocity $\dot{\phi}_1$ (b) of the body I_1. Results obtained with the adaptive scheme of Algorithm 2 and the LQG regulator of Algorithm 3.

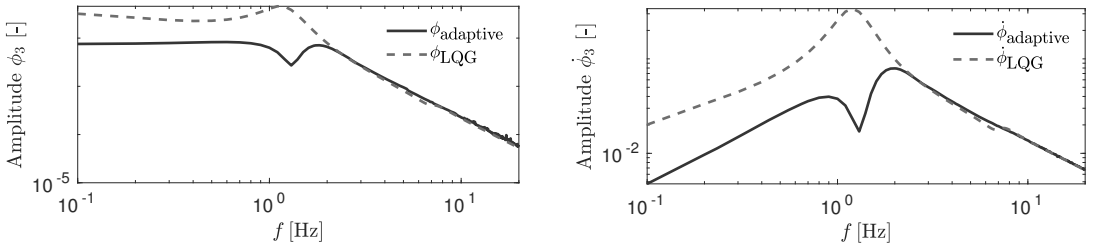

(a) (b)

Fig. 17. Amplitude spectra of the angular deflection ϕ_3 (a) and the angular velocity $\dot{\phi}_3$ (b) of the body I_3. Results obtained with the use of the adaptive scheme of Algorithm 2 and the LQG regulator of Algorithm 3.

greater damping of the oscillations for almost the whole frequency spectrum considered. According to the results, the diagrams can be divided into three regions. For the frequencies lower than 1 Hz, the adaptive control method gives significantly better results than the LQG regulator. The improvement for this interval varies from 10-fold (see

the values depicted in Fig. 16(b) for $f = 0.1$ Hz) to twofold. For the second interval, $f \in [1, 10]$ Hz, the difference between the amplitudes decreases, and for the subinterval $f \in [1, 2.5]$ Hz the LQG regulator results in smaller amplitudes of movement of the body I_1 than in the case of the adaptive scheme. Nevertheless, the body I_3, to which the load is directly applied, still exhibits lower amplitudes for the adaptive control. For the last interval denoted by $f \in [10, 20]$ Hz, responses of both controllers coincide and the adaptive controller exhibits no improvement. The results for the remaining bodies $I_{0,2}$ are similar, but with a noticeable trend: the closer the body to the disturbance, the better the improvement. It may be then concluded that the transitional lack of improvement for the interval $f \in [1, 2.5]$ Hz for the bodies closer to the drive but farther from the disturbance is a result of the adaptive scheme controlling the motor aggressively to damp out oscillations of the bodies I_{2-3}, more prone to the load.

The favourable results of the analysis for the proposed control scheme come from the fact that the adaptive scheme controls the system using the identification of the linear dynamic model of the load. In this case, the load is a sinusoidal function, which can be precisely approximated by the linear autoregressive model. The fact that the time variation in the disturbance is exactly reconstructed by the model makes the control generated by the adaptive scheme very close to the optimal one.

4.6. Impact of the algorithm parameters. In this section, the effectiveness of the proposed control method is tested for different values of the algorithm parameters: the sample time T_s, the size of the signal window N, the length of the LQR horizon T_{horizon}, and the order of the model approximation n. The analysis was performed for the above system set as for the first simulation scenario.

In Fig. 18(a), a comparison of the objective functions computed for different sampling times T_s and different sizes of the window N is presented. One can see that the objective function increases with N. This monotonicity is preserved for different sampling periods T_s. It is important that for $T_N < 1\,\text{s}$, the stabilization of the dynamic system fails. A signal horizon shorter than $1\,\text{s}$ is not sufficient to calculate a good autoregressive approximation of the torque dynamics. This critical value of T_N is related to the system configuration described above. For a system governed by different dynamic equations or with frictions of different characteristics, this value will naturally be different. However, it appears that the value of J_x as a function of T_s does not change monotonically. The lowest characteristics presented in Fig. 18(a) are computed for $T_s = 0.007\,\text{s}$. The next one is computed for the shorter sampling period $T_s = 0.006\,\text{s}$. This trend breaks as the characteristics for $T_s = 0.004\,\text{s}$ and $T_s = 0.003\,\text{s}$ show lower values of J_x than the characteristics computed for $T_s = 0.005\,\text{s}$. This phenomenon is presented in Fig. 18(b), where the values of the objective function J_x are computed for a fixed length of the window T_N and different sampling periods T_s. One can notice that, although the characteristics are not smooth (which explains the seeming randomness of the results in Fig. 18(a)), the global trend is that the value of the objective function increases with an increase in the sampling period. However, a reduction in the sampling period T_s involves an increase in the window size N. This ensures acceptable control results in the unchanged horizon of the measurements $T_N = N \cdot T_s$. The increase in N results in a longer execution time of the proposed algorithm. This means that there is a critical value of T_s below which the execution time of the algorithm exceeds the sampling time and the algorithm fails to be useful in real time.

Figure 19(a) presents the influence of the value of the LQR horizon on the objective function. For short T_{horizon}, e.g., $T_{\text{horizon}} < 0.5\,\text{s}$, the algorithm fails. For longer simulation times, the value of the objective function calculated for $T_{\text{horizon}} < 0.5\,\text{s}$ will be higher, but for $T_{\text{horizon}} \geq 0.5\,\text{s}$ it will remain still, as the adaptive algorithm stabilizes the system in the simulation time. For $T_{\text{horizon}} > 0.5\,\text{s}$ one can observe that the value of the function stabilizes, and for $T_{\text{horizon}} > 1\,\text{s}$ there is no profit in a further increase in the horizon.

In Fig. 19(b) the prediction ability of the AR model used in the derived algorithm is presented. The reference signal of the friction torque (in Fig. 19(b) referred to as "measurement") that was used to analyze the AR models was computed from the results of the first simulation case presented in Section 4.1. The signal "measurement" is a friction torque generated by the model (1) represented in the error space defined in (20) with the use of the parameters from Table 2 and the angular velocity of the last body $\dot{\phi}_3$ measured at the first simulation case, i.e., $\text{measurement}(t) = T_F^{\epsilon}(\dot{\phi}_3(t))$.

Then the AR models were generated with various values of the parameter n. The predicted future signals of these models are compared with the values of the torque calculated in the simulation. The other parameters of the proposed algorithm are as in the previous cases. One can see that the order of the autoregressive model $n = 1$ is too low to give a good prediction of the signal because dynamical models of order 1 cannot reproduce oscillations. With the order equal to $n = 2$ or larger, the oscillations are properly approximated by the model. However, the increase in the order to $n = 3$ provides a better approximation of the original signal; the overall change compared with $n = 2$ is small. In addition, a further increase in the order to $n > 3$ does not provide a significant change in the quality of the approximation.

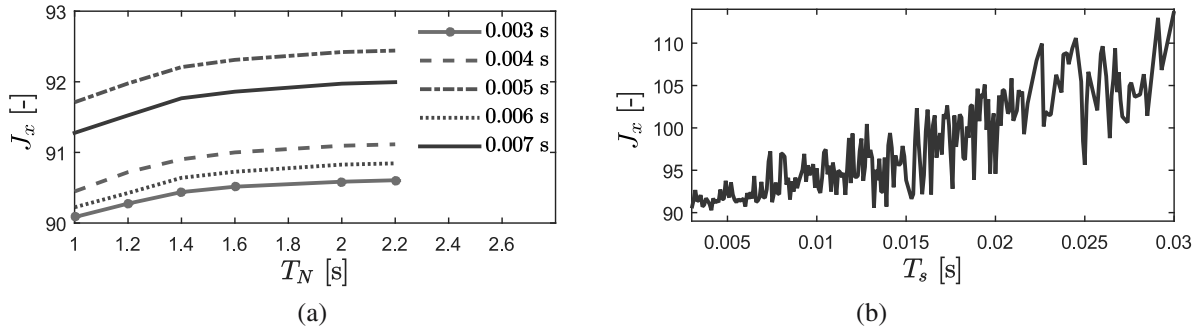

(a) (b)

Fig. 18. Dependence of the objective function achieved by the adaptive controller of Algorithm 2 on the parameters: comparison of the objective functions achieved by the adaptive controller for different sampling periods T_s and different lengths of the window T_N ($T_N = N \cdot T_s$) (size of the LQR horizon is constant, $T_{\text{horizon}} = 1.5\,\text{s}$) (a), objective function as the function of the sampling period T_s (order of the disturbance model $n = 3$, size of the window $T_N = 1.5\,\text{s}$, sampling period) (b).

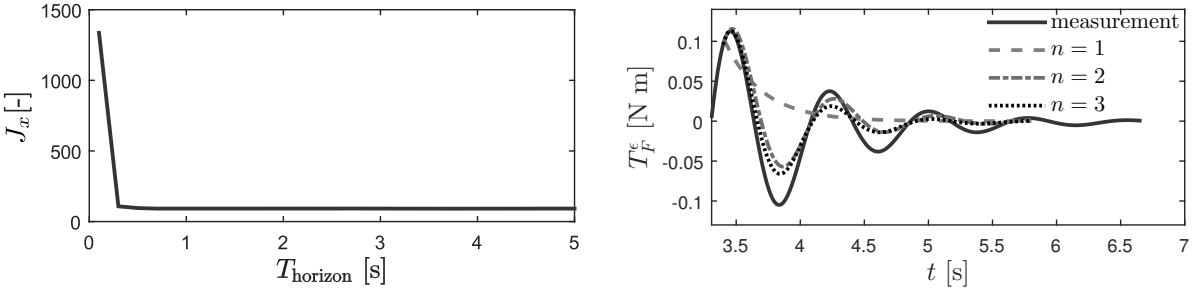

(a) (b)

Fig. 19. Influence of selected parameters on the control quality: impact of the length of the horizon T_{horizon} (a), ability of the disturbance prediction for different orders n of the model ($N = 220$) (b).

4.7. Impact of the number of elements. In Section 4 the developed control algorithm was tested on a system consisting of four rigid bodies. However, a real drilling machine is comprised of a long drill string, which is an example of a distributed parameter system. To check if the control scheme can be successfully used in a real scenario, the efficiency of the control of the model with an increased number of elements is investigated. Such a modification provides a more accurate model of a real system.

The control algorithm is computed as previously by using the simplified model described in Section 2. The control is then applied to the altered model, consisting of a greater number of interior elements. The scheme of the model is presented in Fig. 20.

The parameters: linear density ρ, shear modulus G, torsion inertia moment I, torsional damping coefficient c and length l of the interior body were selected so that they correspond to the parameters I_1, I_2, k_1, k_2, c_1, c_2 of the simplified model described in Section 2. Measurements of the angular displacements and angular velocities corresponding to the interior bodies of the simplified model were made at the $1/3$ and $2/3$ of the length of the interior body.

The simulation scenario described in Section 4.1 was then performed for the interior body I discretized using 1–11 elements (the case with discretization using one element is identical to the model from Section 2). To measure the performance of the scheme, a quadratic performance index defined by (44) for the altered model was introduced. The indices of the diagonal matrix Q corresponding to the elements of the interior body are inversely proportional to the number of elements, to ensure normalization of the cost function. For all cases, the control scheme successfully steers the system to the angular velocity set point.

The final value of the cost function as the function of the number of elements is presented in Fig. 21. As can be observed, the initial increase up to the three elements makes the performance index deteriorate. The peak corresponds to 150% of the performance index for only one element. However, a further increase in the elements makes the performance index decrease. The final value for the choice of 11 elements is approximately 25% higher than for the one-element model. It has been validated that a further increase in the number of elements does not significantly affect the value of the performance index. This result confirms that the developed control scheme can be successfully used in a real-world application with

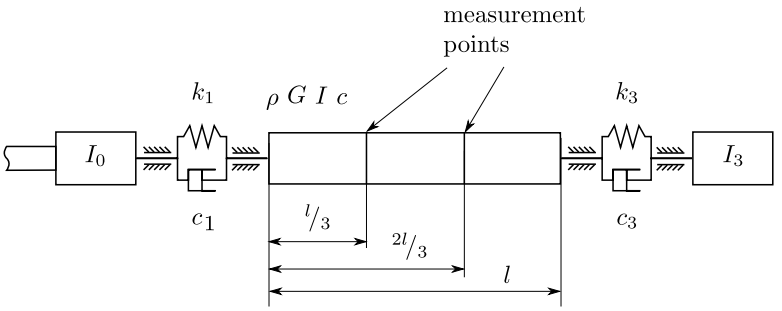

Fig. 20. Scheme of the altered model with the points on which the measurements are conducted.

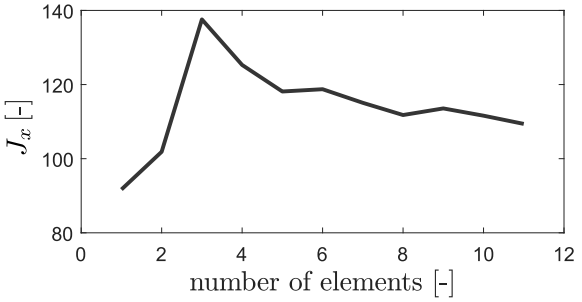

Fig. 21. Value of the performance index J_x for different numbers of elements in the model.

only two additional measurements of the displacement and velocity on the drill string.

5. Conclusions

In this paper, an optimal adaptive controller for dynamical systems with external disturbances was studied. The proposed scheme was applied to the control problem of a drill string. Simulations proved the efficiency of the approach. It successfully steers the system to the desired trajectory. The proposed control method is efficient in the presence of suddenly varying and nonlinear disturbances. The numerical simulations demonstrated that the described controller is superior to the linear quadratic Gaussian control in the given control case. The scheme is robust to changing characteristics of the friction and the presence of noise. The performed simulations confirmed that the adaptive scheme can control a system subjected to multiple independent disturbances. The scope of the application of the scheme can be easily enlarged to the cases where the disturbance is independent of the state of the system.

The method is versatile and can be applied to numerous engineering problems, for example, the stabilization of off-road vehicles subjected to sudden unevenesses of the surface, the stabilization of airplane wings under turbulence, masts under wind blows, slender buildings under seismic excitation or satellite antennas impacted by meteorites.

Acknowledgment

This research has been supported by the National Science Centre, Poland, under the grant agreements UMO-2015/17/B/ST8/0324 and DEC-2017/26/D/ST8/00883.

References

Alin, A. (2010). Multicollinearity, *Wiley Interdisciplinary Reviews: Computational Statistics* **2**(3): 370–374, DOI: 10.1002/wics.84.

Bailey, J.R. and Remmert, S.M. (2010). Managing drilling vibrations through BHA design optimization, *SPE Drilling & Completion* **25**(4): 458–471, DOI: 10.2118/139426-PA.

Bajer, C.I., Pisarski, D., Szmidt, T. and Dyniewicz, B. (2017). Intelligent damping layer under a plate subjected to a pair of masses moving in opposite directions, *Journal of Sound and Vibration* **394**: 333–347, DOI: 10.1016/j.jsv.2017.01.046.

Christoforou, A.P. and Yigit, A.S. (2003). Fully coupled vibrations of actively controlled drillstrings, *Journal of Sound and Vibration* **267**(5): 1029–1045, DOI: 10.1016/S0022-460X(03)00359-6.

Davis, J.E., Smyth, G.F., Bolivar, N. and Pastusek, P.E. (2012). Eliminating stick-slip by managing bit depth of cut and minimizing variable torque in the drillstring, *IADC/SPE Drilling Conference and Exhibition, San Diego, CA, USA*, pp. 402–410, DOI: 10.2118/151133-MS.

Farrar, D.E. and Glauber, R.R. (1967). Multicollinearity in regression analysis: The problem revisited, *The Review of Economics and Statistics* **49**(1): 92–107, DOI: 10.2307/1937887.

Fear, M.J. and Abbassian, F. (1994). Experience in the detection and suppression of torsional vibration from mud logging data, *European Petroleum Conference, London, UK*, pp. 433–448, DOI: 10.2118/28908-MS.

Hernandez-Suarez, R., Puebla, H., Aguilar-Lopez, R. and Hernandez-Martinez, E. (2009). An integral high-order sliding mode control approach for stick-slip suppression in oil drillstrings, *Petroleum Science and Technology* **27**(8): 788–800, DOI: 10.1080/10916460802455483.

Hillsley, K.L. and Yurkovich, S. (1991). Vibration control of a two-link flexible robot arm, *1991 IEEE International Conference on Robotics and Automation, Sacramento, CA, USA*, Vol. 3, pp. 212–216, DOI: 10.1109/ROBOT.1991.131941.

Jansen, J.D. and van den Steen, L. (1995). Active damping of self-excited torsional vibrations in oil well drillstrings, *Journal of Sound and Vibration* **179**(4): 647–668, DOI: 10.1006/jsvi.1995.0042.

Kar, I.N., Miyakura, T. and Seto, K. (2000a). Bending and torsional vibration control of a flexible plate structure using H_∞-based robust control law, *IEEE Transactions on Control Systems Technology* **8**(3): 545–553, DOI: 10.1109/87.845884.

Kar, I.N., Seto, K. and Doi, F. (2000b). Multimode vibration control of a flexible structure using H_∞-based robust control, *IEEE/ASME Transactions on Mechatronics* **5**(1): 23–31, DOI: 10.1109/3516.828586.

Kreuzer, E. and Steidl, M. (2012). Controlling torsional vibrations of drill strings via decomposition of traveling waves, *Archive of Applied Mechanics* **82**(4): 515–531, DOI: 10.1007/s00419-011-0570-8.

Kucuk, I., Yildirim, K., Sadek, I. and Adali, S. (2013). Active control of forced vibrations in a beam via Maximum principle, *2013 5th International Conference on Modeling, Simulation and Applied Optimization (ICMSAO), Hammamet, Tunisia*, pp. 1–4, DOI: 10.1109/ICMSAO.2013.6552558.

Li, X., Agarwal, R.K. and Shue, S.-P. S.-P. (1994). Optimal control and H_∞ filter for control of Timoshenko beam vibrations using piezoelectric material, *Proceedings of the 37th IEEE Conference on Decision and Control, Tampa, FL, USA*, Vol. 2, pp. 1566–1571, DOI: 10.1109/CDC.1998.758513.

Michajłow, M., Jankowski, Ł., Szolc, T. and Konowrocki, R. (2017). Semi-active reduction of vibrations in the mechanical system driven by an electric motor, *Optimal Control Applications and Methods* **38**(6): 2–8, DOI: 10.1002/oca.2297.

Mihajlović, N., van Veggel, A.A., van de Wouw, N. and Nijmeijer, H. (2004). Analysis of friction-induced limit cycling in an experimental drill-string system, *Journal of Dynamic Systems, Measurement, and Control* **126**(4): 709–720, DOI: 10.1115/1.1850535.

Mohamed, Z., Chee, A.K., Hashim, A.W.I.M., Tokhi, M.O., Amin, S.H.M. and Mamat, R. (2006). Techniques for vibration control of a flexible robot manipulator, *Robotica* **24**(4): 499–511, DOI: 10.1017/S0263574705002511.

Monteiro, H.L.S. and Trindade, M.A. (2017). Performance analysis of proportional-integral feedback control for the reduction of stick-slip-induced torsional vibrations in oil well drillstrings, *Journal of Sound and Vibration* **398**: 28–38, DOI: 10.1016/j.jsv.2017.03.013.

Orlowska-Kowalska, T., Kaminski, M. and Szabat, K. (2010). Implementation of a sliding-mode controller with an integral function and fuzzy gain value for the electrical drive with an elastic joint, *IEEE Transactions on Industrial Electronics* **57**(4): 1309–1317, DOI: 10.1109/TIE.2009.2030823.

Pisarski, D. and Bajer, C.I. (2010). Semi-active control of 1D continuum vibrations under a travelling load, *Journal of Sound and Vibration* **329**(2): 140–149, DOI: 10.1016/j.jsv.2009.09.006.

Pisarski, D. and Canudas-de-Wit, C. (2016). Nash game-based distributed control design for balancing traffic density over freeway networks, *IEEE Transactions on Control of Network Systems* **3**(2): 149–161, DOI: 10.1109/TCNS.2015.2428332.

Pisarski, D. and Myśliński, A. (2017). Online adaptive algorithm for optimal control of structures subjected to travelling loads, *Optimal Control Applications and Methods* **38**(6): 1168–1186, DOI: 10.1002/oca.2321.

Priesner, R. and Jakubek, S. (2014). Mechanical impedance control of rotatory test beds, *IEEE Transactions on Industrial Electronics* **61**(11): 6264–6274, DOI: 10.1109/TIE.2014.2308159.

Serrarens, A.F.A., Van De Molengraft, M.J.G., Kok, J.J. and Van Den Steen, L. (1998). h_∞ control for suppressing stick-slip in oil well drillstrings, *IEEE Control Systems Magazine* **18**(2): 19–30, DOI: 10.1109/37.664652.

Singhose, W. (2009). Command shaping for flexible systems: A review of the first 50 years, *International Journal of Precision Engineering and Manufacturing* **10**(4): 153–168, DOI: 10.1007/s12541-009-0084-2.

Symans, M.D. and Constantinou, M.C. (1999). Semi-active control systems for seismic protection of structures: a state-of-the-art review, *Engineering Structures* **21**(6): 469–487, DOI: 10.1016/S0141-0296(97)00225-3.

Szabat, K., Tran-Van, T. and Kaminski, M. (2015). A modified fuzzy Luenberger observer for a two-mass drive system, *IEEE Transactions on Industrial Informatics* **11**(2): 531–539, DOI: 10.1109/TII.2014.2327912.

Tzes, A. and Yurkovich, S. (1993). An adaptive input shaping control scheme for vibration suppression in slewing flexible structures, *IEEE Transactions on Control Systems Technology* **1**(2): 114–121, DOI: 10.1109/87.238404.

van de Vrande, B.L., van Campen, D.H. and de Kraker, A. (1999). An approximate analysis of dry-friction-induced stick-slip vibrations by a smoothing procedure, *Nonlinear Dynamics* **19**(2): 159–171, DOI: 10.1023/A:1008306327781.

Wang, S., Ren, X. and Na, J. (2016). Adaptive dynamic surface control based on fuzzy disturbance observer for drive system with elastic coupling, *Journal of the Franklin Institute* **353**(8): 1899–1919, DOI: 10.1016/j.jfranklin.2016.03.006.

Young, K. (1998). A polar coordinate based sliding mode design for vibration control, *IEEE International Workshop on Variable Structure Systems, VSS'96, Tokyo, Japan*, Vol. 8, pp. 181–186, DOI: 10.1109/VSS.1996.578606.

Zhu, X., Tang, L. and Yang, Q. (2015). A literature review of approaches for stick-slip vibration suppression in oilwell drillstring, *Advances in Mechanical Engineering* **6**: 1–17, DOI: 10.1155/2014/967952.

Maciej Wasilewski was born in Lublin, Poland, in 1991. He received his MSc degree in automation and control from the Warsaw University of Technology in 2015. He is currently a PhD student at the Institute of Fundamental Technological Research of the Polish Academy of Sciences. His research interests include designing structural adaptive control algorithms for systems subjected to dynamical changes, numerical analysis of mechanical models, and computational optimization of control.

Dominik Pisarski received the MEng degree in automatic control from AGH University, Cracow, Poland, in 2006. In 2012 he obtained the PhD degree in mechanics from the Institute of Fundamental Technological Research, Polish Academy of Sciences, Warsaw, Poland. In 2014 he obtained the PhD degree in automatic control in the Department of Automatic Control, Grenoble University, France. Since 2014 he has been working as an associate professor in the Department of Intelligent Technologies in the Institute of Fundamental Technological Research, Polish Academy of Sciences. His research focuses on control and optimization of complex mechanical and transportation systems. He is an author of 40 publications, including 16 papers in international journals, 21 international conference papers, 1 book and 2 book chapters.

Robert Konowrocki was born in Poland in 1975, and received the MSc degree in mechanics from the Warsaw University of Technology (Faculty of Automotive and Construction Machinery Engineering) and the PhD degree in construction and operation of machines from IPPT PAN in 2002 and 2007, respectively. In 2007 he took an assistant professor position with the Department of Control and System Dynamics (IPPT PAN). His main research activities include experimental and simulation analysis of railway infrastructure vibration, development of measurement methods and monitoring, and assessment of civil constructions. His recent areas of research investigation of the dynamic electromechanical coupling effects in machine and vehicle drive systems. As of 2014, he is also an expert of the Polish National Centre for Research and Development and the Polish Agency for Enterprise Development.

Czesław I. Bajer received the MSc degree in civil engineering from the University of Zielona Góra (Poland), the PhD degree in civil engineering from the Warsaw University of Technology, and the DSc degree in mechanical engineering from the Institute of Fundamental Technological Research, Polish Academy of Sciences (Warsaw). He has worked at the University of Lorraine (France), the University of Clermont-Ferrand II (France) and the University of Perpignan (France). In 2010 he received a professorial title. He is a full professor of technical sciences at the Institute of Fundamental Technological Research. His current research interests include structural dynamics, computational methods in engineering, and smart and controlled structures.

Received: 4 April 2018
Revised: 21 December 2018
Re-revised: 22 February 2019
Accepted: 2 March 2019